Adeno-associated viral capsid stability on anion exchange chromatography column and its impact on empty and full capsid separation

Ohnmar Khanal,[1,2] Vijesh Kumar,[1,2] and Mi Jin[1]

[1]Technology Development, Spark Therapeutics, Inc., Philadelphia, PA, USA

Recombinant adeno-associated viral vector (rAAV) mediated gene therapy is gaining traction in treating genetic disorders. Current rAAV production systems yield a mixture of capsids largely devoid of the transgene (empty capsid) compared with the desired therapeutic product (full capsid). Anion exchange chromatography (AEX) is an attractive method for separating empty and full AAV capsids because of its scalability. Resin types and buffer composition are key considerations for AEX and must support capsid stability to be suitable for downstream processing. We examined the impact of binding durations (0–8 h) using various binding ionic strengths (15–75 mM), pH (7.5–9.0), resin chemistry (POROS XQ, POROS HQ, POROS I, and BIA QA monolith), and proprietary Q resins with different ligand densities for effects on capsid stability. Empty capsids were altered upon extended binding, leading to retention time shifts and loss of resolution between empty and full capsids. Viral capsid protein analysis reveals that full capsids have more viral capsid protein 3 (VP3) proteins than empty capsids. Analytical hydrophilic liquid chromatography showed that empty capsid retention time shift is accompanied by changes to the empty capsid's native VP3 protein. Among the potential stabilizing additives considered, magnesium chloride was the most effective at reducing negative impacts caused by extended binding.

INTRODUCTION

Gene therapy involves the administration of exogenous genes to the patient to alter gene or protein expression.[1] Gene therapy is suited for treating inherited genetic disorders and holds promise in treating an increasing number of diseases, such as hereditary blindness,[2] hemophilia,[3] neurodevelopmental disorders,[4] and neurodegenerative diseases.[5] An estimated 2,000 gene therapies are in development globally as of 2022.[6] Among the available vehicles for therapeutic gene delivery, recombinant adeno-associated viral vectors (rAAVs) are currently the leading platform because of their relative safety and efficacy in humans.[7,8]

A major challenge in AAV-mediated gene therapy manufacturing is the low productivity and high cost. Additionally, rAAV production processes often yield a heterogeneous array of product-related impurities, such as rAAV capsids fragmented or absent transgene; these impurities can ultimately increase the administered capsid burden. Until recently, the large-scale separation of empty and full capsids was challenging; clinical investigations were commenced[9] with therapeutics comprising a mixture of empty and full capsids.

The safety and efficacy of AAV-mediated gene therapy[10,11] can be disrupted through a number of mechanisms.[12] Naturally occurring antibodies toward AAVs can be found in humans[13] through natural infections. High-dose intravitreal injection of AAV2 capsids into the eye has increased anti-AAV antibodies and triggered anti-capsid T cell responses.[14] Excess empty particles may also trigger T cell response, causing cytotoxicity and partial loss of expression.[11] Because of these concerns, a robust method to separate empty capsids from transgene-containing capsids is desired to reduce the overall capsid dosage and increase efficiency. Reduced ratios of empty to full capsids have also been shown to improve transduction efficiency for intravenous[15] and intramuscular[16] injection of AAV vectors. In some cases, the ability to tune empty capsid content may be desired, as adding empty particles to the AAV2 drug substance reportedly adsorbed the antibodies and lessened the preexisting humoral immunity to the capsids.[10] Although ongoing studies will continue to inform our desired capsid variant profile in the drug substance, the need for a robust purification strategy and a thorough process understanding to control the product variant profile is paramount. Furthermore, we must ensure that capsid structural integrity is not compromised in scaling the purification process, thus avoiding increased heterogeneity in the final product.

The separation of empty and full capsids can be achieved with ion-exchange chromatography (IEX) across scales and serotypes.[17–22] An increasing number of AAV processes rely on chromatographic purification methods for their scalability and amenability to good manufacturing practice (GMP). IEX has been used to purify AAVs
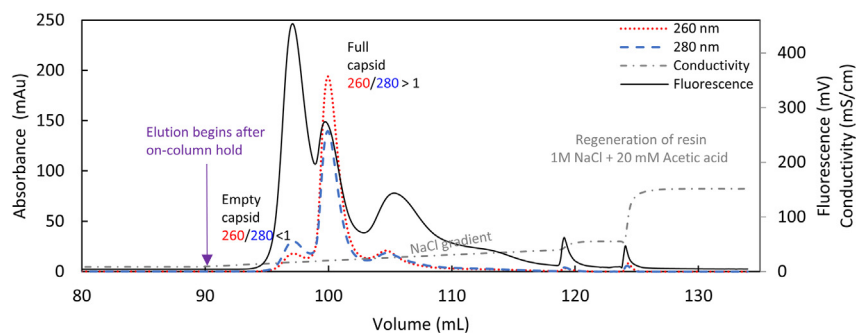
Figure 1. Overlay of fluorescence and absorbance (at 260 and 280 nm) signal-based chromatography profiles

The UV absorbance signals are plotted on the left axis and conductivity, and the fluorescence signals are plotted on the right axis. The purple arrow marks the point in time at which the bound capsids are held on column for a specified period. Irreversibly bound substances are stripped off the column with 1 M NaCl with 20 mM acetic acid at the end of the experiment. The red dotted line and the blue dashed lines represent the absorbance traces at 260 and 280 nm, respectively. The black solid and the gray dash-dotted lines represent the fluorescence and conductivity traces, respectively. The first peak to elute over the sodium chloride gradient is the empty capsids, which absorb more at 280 nm than at 260 nm. The second peak to elute contains primarily transgene-containing capsids, which absorb more at 260 nm than at 280 nm.

for more than two decades.[21–25] Over the past few years, significant improvements in the IEX method development for separating empty and full capsids have been documented[16,17,21,26] with[16] and without[26] additives such as magnesium chloride ($MgCl_2$). Although many have focused on resin selection and buffer optimization to improve separations, few have assessed[21,27–29] on-column[21] or on-resin stability of the capsids. Although the thermal stability of adsorbed foot-and-mouth virus has been correlated to purification recovery,[28] such a study has not been completed for AAVs.

Furthermore, accelerated stability assessments such as thermal stability show challenges in accurately predicting temporal stability.[30–33] The direct evaluation of AAV temporal stability in its adsorbed state during IEX across varying timescales is directly relevant to downstream purification processes and, to the best of our knowledge, has not been reported in the literature. It is advantageous to think about capsid on-column stability in process development to ensure that chromatographic purification does not result in increased product heterogeneity or negatively affect product quality. The binding of AAV capsids to IEX resin occurs in a low-ionic-strength environment that is suitable for promoting higher loading capacities may negatively affect capsid stability.[34] Furthermore, dilution of affinity eluate results in the volume expansion of loading material, necessitating increased loading times and extended binding of rAAV capsids onto the anion exchange chromatography (AEX) resin. Hence, designing a purification strategy that examines product stability in addition to yield and purity is imperative.

A major challenge within the scope of AAV separation with IEX is the concept of product heterogeneity. Although populations of AAV capsids are termed "empty," "partial," or "full" on IEX depending on their retention times, retention times are not solely a function of transgene length but can also shift because of changes in the charge distribution on the capsid proteins.[35,36] In this work, we evaluate the stability of AAV capsids adsorbed onto various anion exchangers, i.e., POROS HQ, POROS XQ, POROS I, POROS D, and BIA QA monolith. Furthermore, we evaluated the impact of AEX resin ligand density on adsorbed protein stability by assessing custom proprietary resins with varying ligand densities.

Although it can be difficult to ascertain the capsid modifications resulting from AAV adsorption to AEX resin in a normal purification process, keeping the AAV adsorbed to the resin for a longer period can magnify the impact of adsorption, allowing us to study on-column capsid stability. In this work, we evaluated the impact of binding AAV capsids to AEX resins for 0–8 h prior to elution. Furthermore, the on-column stability of empty and full capsids was decoupled, revealing disparate stability profiles that raise significant concerns regarding the purity of AEX eluate pools. Several additives were also assessed for their stabilizing or destabilizing impact on-column. Such a comprehensive investigation of rAAV on-column stability across different buffers, additives, resin types, and ligand densities over time and across two recombinant engineered capsids is crucial to purification process development.

RESULTS

Figure 1 shows a preparative AEX chromatogram of rAAVa on CIM-multus QA column recorded with UV, fluorescence, and conductimetric detectors. A linear sodium chloride gradient resolves the capsid variants. In AEX chromatography, the first peak that elutes over the linear salt gradient is mainly the empty capsids, while the second or the subsequent peaks contain the product of interest, as shown in Figure 1. The ratio of UV absorbances at 280 and 260 nm reveals peaks enriched with empty and full capsids. Generally, a peak with a 260/280 ratio of less than one indicates a greater percentage of empty capsids, while a 260/280 ratio greater than one indicates a greater percentage of full capsids.[37–39] More specifically, in the absence of other impurities, 260/280 ratios can indicate the proportion of empty and full capsids in a sample, as reported previously.[40] Given that the extinction coefficient of the rAVVa empty capsid is lower than that of the full capsid by ~9-fold at 260 nm and ~4-fold at 280 nm, the conversion of their peak area to capsid count differs. The native amino acid fluorescence was also monitored using an excitation of 280 nm and emission of 350 nm. Nucleic acid emission at 350 nm is negligible under these conditions; therefore, the relative fluorescence peak areas correspond directly to empty and full capsid counts. The combined fluorescence and absorbance spectra also demonstrate that peaks appearing after the full capsid are more proteinaceous than the full capsids and are present in significant quantity.
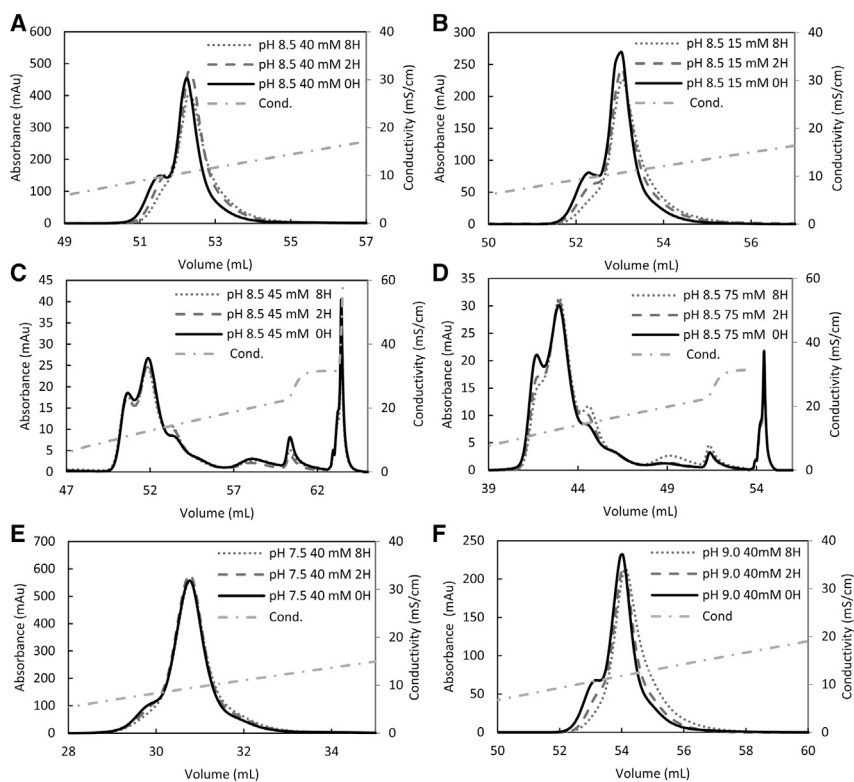
Figure 2. Changes in the chromatographic elution profiles (absorbance at 280 nm) seen after 0–8 h of extended binding in various loading buffer pH and ionic strengths

UV absorbance at 280 nm is plotted on the left axis, and the conductivity trace (dash-dotted line) is plotted on the right axis. (A and B) Loading buffer ionic strengths of 40 mM (A) and 15 mM (B) are presented for rAAVa. (C and D) Loading buffer ionic strength of 45 mM (C) and 75 mM (D) were evaluated for rAAVb. (E and F) The loading pH values of 7.5 (E) and 9.0 (F) at 40 mM are plotted for rAAVa. The black solid, gray dashed, and gray dotted lines represent the chromatographic elution profiles after 0, 2, and 8 h of extended binding, respectively.

The structural integrity of rAAV capsids under AEX chromatographic conditions was assessed by loading affinity chromatography purified capsids onto the POROS XQ column, washing the column, and either eluting the capsids immediately or after an additional 2–8 h of binding. Elution was performed using a linear salt gradient to resolve capsid variants (empty, full, etc.). Such an investigation was carried out for both proprietary capsids rAAVa and rAAVb.

Figure 2A shows that when the rAAVa capsid binds to the POROS XQ at 40 mM ionic strength (IS) for 2 h, the resolution between the empty and full peak is diminished. This effect is exacerbated after 8 h. The empty capsid peak area was reduced (from −0.6% to −38%) over 2–8 h of binding. More pronounced changes (−20% at 2 h and −50% at 8 h) were observed when the rAAVa capsids were bound to the resin at 15 mM IS, as shown in Figure 2B, suggesting that stronger binding to the resin at a lower IS of 15 mM may lead to greater changes in the product quality. The impact of extended binding on the AEX eluate is more clearly seen for rAAVb, for which the drop in peak area at the retention time of the empty capsid is offset by the rise in the third peak (+26% at 45 mM IS and +62% at 75 mM IS). This third peak comprises capsid degradants resulting from on-column instability. Like rAAVa, the extended binding of rAAVb to the POROS XQ resin in a 40–45 mM IS buffer resulted in the least changes to the first peak (−11% after 8 h; Figure 2C). In contrast, at a higher IS of 75 mM IS, changes in the first peak were much more pronounced (−26% after 8 h), as seen in Figure 2D. However, upon binding at 45 mM IS, a larger portion of the rAAVb capsids

bound irreversibly and required 1 M NaCl at pH 3.0 to desorb (resin regeneration peak). No resin regeneration peaks were seen for rAAVa capsid experiments shown in Figures 2A and 2E.

The binding buffer pH's impact on adsorbed capsids' stability was also assessed for rAAVa. The most remarkable changes to the earliest eluting peak area were observed at pH 9 (−59%), followed by pH 8.5 (−50%) and pH 7.5 (−20%) after 8 h. Capsids bind most tightly to the AEX resin at pH 9, significantly destabilizing the adsorbed capsid. Relatively weaker binding at pH 7.5 results in minimal changes to the peak shape and the retention time, as shown in Figures 2A, 2E, and 2F. It is worth noting that although a higher pH leads to greater on-column instability (pH 9; Figure 2F), it also provides a better resolution than at pH 7.5 (Figure 2E).

To further explore the impact of adsorption on the eluate retention time, strong and weak anion exchangers with various ligand chemistry, provided in Table S1, were evaluated. Figure 3 shows the impact of binding rAAVa capsid on POROS I, BIA QA monolith, POROS HQ, and POROS XQ over an additional 0–8 h. Although the resolution between the product variants over the linear NaCl gradient differs for the four anion exchangers, some similarities can be observed. Extended binding onto adsorbents with strong AEX functionality results in the retention time shifting to the right, while extended binding onto POROS PI, a weak anion exchanger, shows a slight shift in the retention time to the left. However, extended binding increases the sample portion lost during elution with a subsequent increase in regeneration peak.

The adsorbent (resin and ligands), the adsorbate (capsids), and the environment (solution) all play a role in the stability of the adsorbed capsids. Following our assessment of two engineered recombinant capsid serotypes and buffers of various pH and ISs, we systematically sought to assess the role of resin ligand density. Apart from the standard POROS XQ resin, custom proprietary Q resins with different ligand densities were provided by Thermo Fisher Scientific. Capsid

on-column stability on these resins was assessed and presented in the left panel in Figure 4. The resin with the highest ligand density, shown in Figure 4A, provided the best resolution between the empty and full capsid at 0 h. The resolution diminishes as the ligand density decreases, as shown in Figures 4C and 4E, making it difficult to discern the impact of extended binding. However, in general, a reduced first peak (or the front side of the elution peak) and an increased third peak (the back side of the elution peak) are still evident.

The simultaneous drop in the first peak and rise in the third peak across different resins and binding strengths, seen in Figures 2A–2F, 3A–3D, 4A, 4C, and 4E, suggests that empty capsids are particularly susceptible to on-column degradation. Empty capsids may be altered over time as they remain bound on the column, resulting in tighter binding and the subsequent shift in the retention time. To test this hypothesis, we purified empty capsids (>90% purity) from full capsids (>90% purity) and evaluated their on-column stability separately. The right panel of Figures 4B, 4D, and 4F shows the changes observed upon binding the empty capsid onto proprietary Q resins of various ligand densities. Comparing the left and right panels of Figure 4 reveals that empty capsids are the major contributor to the rightmost peak that emerges upon extended binding. However, the decrease in the full capsid's peak height over time also signals the destabilization of full capsids. As empty capsids are altered more significantly than full capsids, a period of 6 h was sufficient to show the impact of on-column stability, whereas the mixture of empty and full capsids was bound for 8 h. Furthermore, capsids were kept in solution for 8 h before loading to confirm that capsids were destabilized after adsorption and not before loading onto the column. The retention time and peak shape of the sample held in solution for 8 h are equivalent to that of the sample held in solution for 0 h (Figure S1). Furthermore, the conductivity associated with the retention time of the pure empty and full capsids is the same whether these capsids are loaded separately or as a mixture. The differing retention volumes in the figures are due to different sample loading volumes.

Figure 5A shows the impact of extended binding onto the BIA CIMmultus column for purified empty and full rAAVa capsids separately. Over the linear sodium chloride gradient, three empty capsid variants were resolved, while the full capsid eluted as one prominent peak. Extended binding of the empty capsid led to the rise of the empty capsid variants 2 and 3, marked as E2 and E3, and the subsequent loss of empty capsid variant 1, marked as E1. Extended binding of full capsids led to the slight shortening and broadening of the peak. Figure 5B shows the impact of extended binding onto the same monolith column for a capsid preparation comprising both empty and full capsids. Similar to what is observed in Figure 5A, extended binding leads to a rise in the third peak and a subsequent decline in the area of the first peak or the empty peak. The empty and full capsid variants were compared through the separation and analysis of their viral capsid proteins (VPs) using an amide-bonded hydrophilic interaction liquid chromatography (HILIC) column, following an established[41] method. The viral protein variants detected using the HILIC are shown in Figures 5C and 5D. The stoichiometry of VPs 1, 2, and 3 was determined (Figure 5E) by integrating their respective peak areas. Two solid lines that denote the commonly accepted VP1/VP2/VP3 ratio of 1:1:10 are provided for reference. Figure 5F shows that VP3 protein variants are present in different amounts among the empty and full capsid variants. The variant VP3.2, which elutes after the main VP3 variant, is seen in empty capsids but not in full capsids. Figure 5G shows that VP1 and VP2 protein variants are present in variable amounts among the empty and full capsid variants. Figures 5H and 5I show the overlay of the hydrophilic liquid interaction chromatograms of the early and later eluting empty (Figure 5H) and combination capsids (Figure 5I) from AEX. Figure 5H shows that the later eluting empty peaks E2 and E3 consist of greater percentages of VP3.2 and VP3.3, compared with the earlier eluting peak E1.

Given that both adsorbed rAAVa and rAAVb capsids destabilized over time on the AEX resin, albeit to different extents, mitigatory measures were sought. Additives such as glycerol, Kolliphor P188, $(NH_4)_2SO_4$, and $MgCl_2$ were added to the rAAVa sample, prior to loading onto the column, and included in the equilibration and wash buffers but not in elution buffers. Figure 6A shows the control
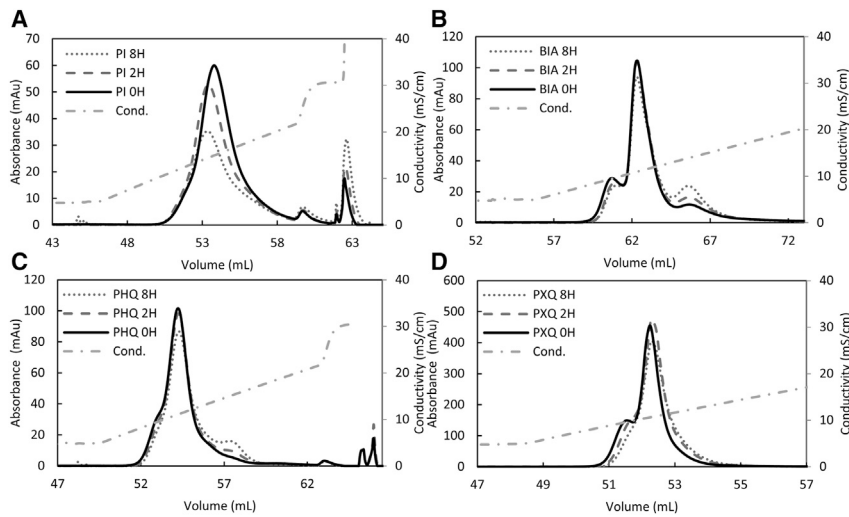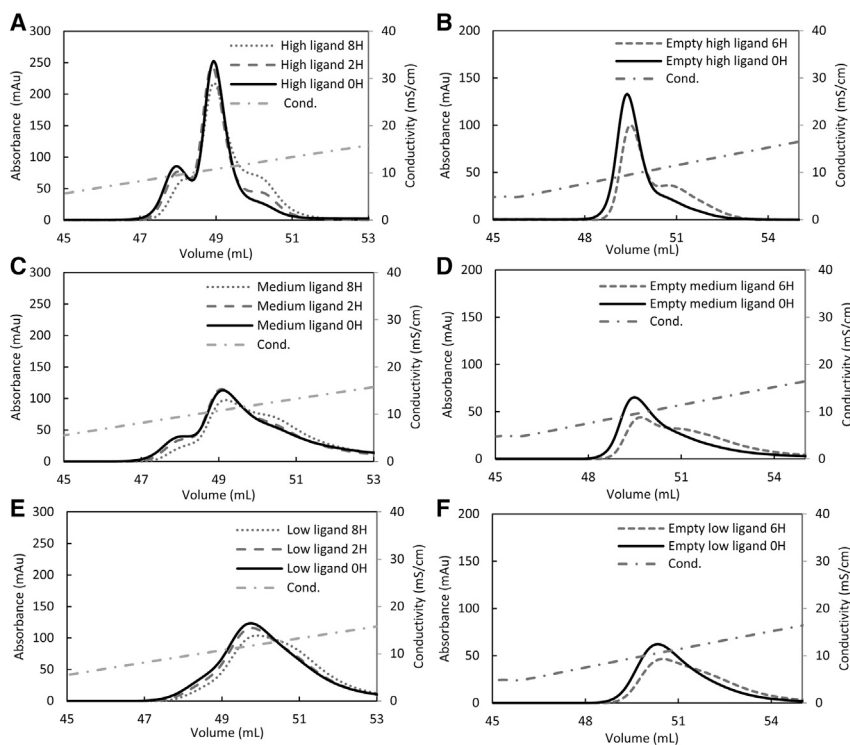
Figure 4. Changes in the chromatographic elution profile (absorbance at 280 nm) were seen after 0–8 h of extended binding onto proprietary Q resin of various ligand densities

UV absorbance at 280 nm is plotted on the left axis, and the conductivity trace (dash-dotted line) is plotted on the right axis. (A–F) Chromatographic elution traces are shown on proprietary Q high (A and B), medium (C and D), and low ligand density (E and F) resins. The left panel shows the chromatographic profile for empty and full capsid mixture, while the right panel shows that for empty capsids alone. The black solid, gray dashed, and dotted lines for the left panel represent the chromatographic elution profiles after 0, 2, and 8 h of extended binding, respectively. For the right panel, the black solid and the gray dashed lines represent the chromatographic elution profiles after 0 and 6 h of extended binding, respectively.

chromatograms on POROS XQ without any additive, while Figures 6B, 6C, and 6D show the impact of 5% glycerol, 0.003% Kolliphor P188, and 15 mM $(NH_4)_2SO_4$, respectively. Glycerol and Kolliphor P188 did not prevent the changes that occur over time on the column for rAAVa. In the presence of $(NH_4)_2SO_4$, the full capsid peak shape changed minimally after 8 h of extended binding, demonstrating its utility. However, empty capsid stability could not be evaluated because empty capsids did not bind upon adding 15 mM $(NH_4)_2SO_4$.

Finally, the impact of $MgCl_2$ on the stability of rAAVa capsid in its adsorbed state was assessed. Without $MgCl_2$ (Figure 7A), the empty and full peaks are altered, albeit with a different amount, after an 8 h on-column hold, aligned with observations presented in Figures 2, 3, and 4. However, no changes to the rAAVa full capsid's eluate peak area, shape, and retention time were observed upon adding 5 mM $MgCl_2$ (Figure 7B). $MgCl_2$ also stabilized the empty capsids significantly, leading to minimal changes even after 8 h of extended binding (Figure 7C). For a more sensitive assessment, the intrinsic fluorescence from the empty capsids, presented in Figure S2, shows that while a right shoulder does develop in the presence of $MgCl_2$ (Figure S2B), it is minute compared with that seen in the absence of $MgCl_2$ in Figure 6A. Although 5 mM $MgCl_2$ is ideal for preserving the adsorbed capsid stability for numerous hours, on-column degradation is mitigated even in the presence of 2.5 mM $MgCl_2$, as shown in Figure 7D. A concentration greater than 5 mM of $MgCl_2$ was not assessed, as it would increase the overall sample IS and would not be favorable for the binding of the empty capsids at 40 mM NaCl.

DISCUSSION

A typical purification process for rAAVs begins with an affinity chromatography step, which uses selective affinity ligands to capture rAAV particles from the harvest lysate, followed by an AEX step to enrich for full capsids. Elution from the affinity column is achieved using a low pH buffer, which is promptly neutralized with suitable buffers to a desired pH and IS to ensure capsid stability. Binding to the AEX resin occurs at a lower IS and the affinity eluate often needs to be substantially diluted to meet a lower IS criterion for binding onto the AEX resin. The use of higher buffer IS (>150 mM) to promote AAV stability[29,34] is well known, raising concerns about adsorbed vector stability during the AEX chromatographic purification. Furthermore, larger loading volumes, a consequence of the post-affinity dilution step, require longer loading times and result in the extended duration of AAV capsids on the AEX resin. We sought to understand the impact of extended binding times at low IS on the eluate product quality and changes to heterogeneity.

Although changes to product heterogeneity are not yet well understood for AAVs, similar lessons can be learned from other therapeutics, such as monoclonal antibodies (mAbs), in which product heterogeneity can arise from post-translation modification and degradation events. These aberrations can affect product stability and biological function[42] and product variants will have altered chromatographic separation on AEX, as evidenced by retention time shifts.[42,43] Some studies have reported the presence of capsid variant peaks in AEX that are in addition to empty and full capsid peaks, the size of which depended upon the composition of the sample loading buffer.[21,37] This additional capsid variant peak displayed greater polydispersity than the main full capsid variant,[37] indicating that certain facets of AAV capsid heterogeneity can be resolved using AEX.

The impact of extended binding is manifested in a loss of the first peak area and the subsequent broadening of the second peak, resulting in the
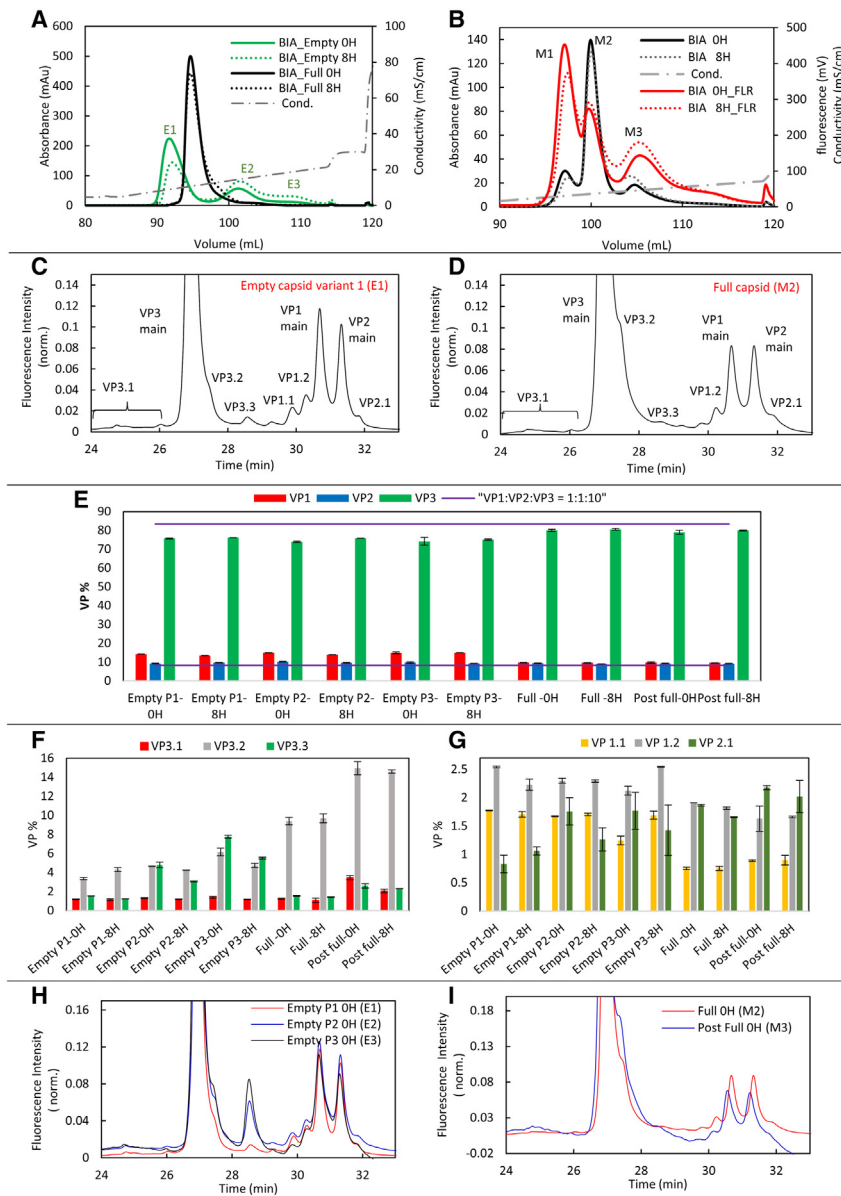
Figure 5. Comparing the rAAVa empty and full capsid variants and the viral protein compositions

(A) Pure empty and full rAAVa capsids 0–8 h on-column hold were resolved across a linear sodium chloride gradient on the BIA monolith column. (B) Changes in the chromatographic elution profile were seen after 0–8 h of extended binding of a mixture of empty and full capsids. The UV absorbance signals are plotted on the left axis, and conductivity and the fluorescence signal are plotted on the right axis. Solid and dotted lines represent the chromatographic elution profiles after 0 and 8 h of extended binding, respectively. (C and D) Separation of rAAVa empty (E1) capsid and full (M1) capsids viral proteins using an amide-bonded, hydrophilic interaction analytical column. (E) Variation in viral capsid protein ratios among empty and full capsid variants. (F and G) Variation in the percentage of VP3 (F) and VP1 and VP2 (G) capsid protein variants. (H and I) Overlay of hydrophilic interaction chromatograms for empty (H) and full capsid variants (I), depicting the differences in VP3 composition. The data plotted in figures E, F, and G are the mean percentages taken from two data sets, and the error bars depict the standard deviations.

ibly bound capsid can be only eluted out in the resin regeneration step. This finding demonstrates that weaker binding is preferred to preserve capsid integrity on the column and that instability can still ensue at a higher IS for capsid variants that are susceptible to irreversible binding. The assessment of binding buffer pH (Figures 2A, 2E, and 2F) reinforces the observation that weaker binding of the capsid leads to better stability in the adsorbed state, as binding at pH 7.5 resulted in minimal changes over time, followed by pH 8.5 and 9. However, binding at pH 7.5 is not practical for rAAVa as the resolution between the empty and full capsid is diminished.

Apart from the binding buffer's IS and pH, the adsorbent also affects the binding event. To this end, the impact of extended binding on anion exchangers with various resin chemistries and ligand densities described in Table S1 was evaluated. It is worth noting that although all the POROS resins evaluated in this study are of 50 μm particle size, the differing base bead chemistry and ligand densities dictate the average pore size. For example, while the standard bead pore size is reportedly between 100 and 360 nm, the pore will be further hindered or unhindered with increasing or decreasing ligand densities. Better accessibility to the pore space broadens the eluate peaks as capsids can sample more pore space. Therefore, the eluate peak shape and area can only be directly compared between the 0 and 8 h hold samples for each resin. Despite this caveat, apart from POROS PI, all the anion exchangers evaluated in this study either showed a shift in the retention time to the right or a concomitant loss of area in the first peak and rise in the last peak

merging of empty and full capsids into one broad peak. Loss of resolution between the empty and full capsids because of extended binding makes the task of separating empty from full capsid challenging. Lowering the binding IS from 40 to 15 mM (Figures 2A and 2B) resulted in an additional 12% reduction in rAAVa empty peak area after 8 h, signifying that stronger binding leads to greater retention time shifts and greater heterogeneity in the capsids. A more degradation-prone capsid, rAAVb, was also evaluated (Figures 2C and 2D). Although binding rAAVb capsids onto the POROS XQ resin at 45 mM IS resulted in a lower recovery (70%) compared with that at 75 mM IS (85%), fewer changes in the eluate were observed over time. Although a larger fraction of the rAAVb capsids bound irreversibly at 45 mM IS, the reversibly bound fraction did not undergo significant changes over 0–8 h. Irrevers-
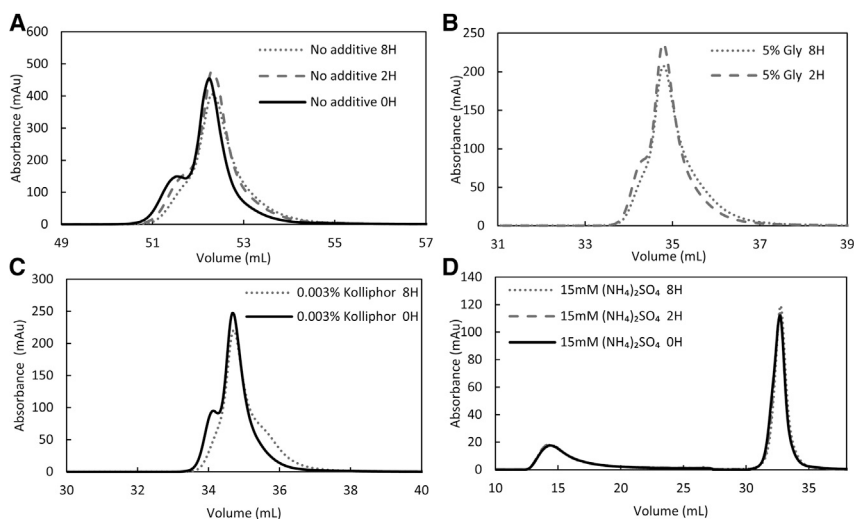
Figure 6. Changes in the chromatographic elution profiles (absorbance at 280 nm) of rAAVa seen after 0–8 h of extended binding onto POROS XQ resin in the presence or absence of additives

UV absorbance at 280 nm is plotted. (A–D) Elution chromatogram generated in the absence of additives is shown in (A), while those in the presence of 5% glycerol, 0.003% Kolliphor P188, and 15 mM $(NH_4)_2SO_4$ are shown in (B), (C), and (D), respectively. The black solid, gray dashed, and gray dotted lines represent the elution chromatographic profiles after 0, 2, and 8 h of extended binding, respectively. The dash-dotted line in (D) represents the elution chromatogram obtained when a sample held at room temperature (RT) for 8 h is loaded onto the column, washed, and eluted from the column immediately.

area (Figures 3 and 4). The proprietary Q resin with high ligand density clearly shows the loss of the empty peak area and a subsequent rise of the third peak area. Regardless of the resolution, the impact of extended binding is seen across resin of all ligand densities, suggesting that de-crowding of the adsorbed capsid on the resin surface does not promote on-column stability.

Extended binding of the rAAVa capsid on the POROS resin leads to on-column degradation of the capsids, a reduction in standard peaks and the emergence of an impurity peak. Empty capsids are the most susceptible to on-column degradation; the parallel assessment of on-column and in-solution empty capsid age (8 h) revealed that the extended binding to the resin destabilizes the empty capsids. Furthermore, purified full capsids retained homogeneity, even after extended binding, signifying their superior on-column stability compared with empty capsids (Figures 5A and 7A).

The green absorbance trace at 280 nm in Figure 5A clearly shows that a large portion of empty capsids binds more strongly to the resin after 8 h of extended binding. The changes observed for the full capsids (black trace) are minor compared with that of the empty capsid, suggesting that full rAAVa capsids are more stable in their adsorbed state than their empty counterpart. A fluorescence detector was paired with the AKTA to increase sensitivity and further discern changes not seen by the UV detector. Figure S2 shows the intrinsic fluorescence from the full capsids. The analytical AEX characterization of each peak fraction is also presented in Figure S3. Empty capsid peaks E2, E3, and mixture peak M3 show an increase in peak area after 8 h of extended binding, consistent with the finding on the preparative AEX column. Although we have not tested the functionality of the tighter binding species that grow with on-column hold time, the demonstrated tighter binding to the AEX indicates a gain of a negative charge or a reduction in the isoelectric point of the VP(s). Prior work[36] has shown that more negatively charged VPs with a greater percentage of deamidation bind more tightly on AEX and have a lower potency.[44]

To further probe the differences between the empty (E1, E2, and E3) and full (M2) capsid variants, these capsid variant fractions were analyzed for their VP composition on the HILIC analytical column. A comparison of Figures 5C and 5D shows that empty and full capsids differ in their VP1/VP2/VP3 ratios. Empty capsids contain a greater percentage of VP1 and a lower percentage of VP3 than full capsids, as shown in Figure 5E. The first peak of the mixture M1 (empty), also follows the same trend for VP ratio and its variants when compared with pure empty capsid peak E1, indicating that differences observed for VP ratio and its variants do not arise from sample preparations. A recent mass spectrometry study showed that capsid assembly is highly variable and stochastic in nature.[45] Here, we report a systematic discrepancy in VP ratios among empty and full capsids. Our findings also show that empty viral capsids display lower stability in the adsorbed state and are structurally different from full ones. The HILIC resolves several variants of the VP3 protein (Figures 5C and 5D), the most abundant VP. Analysis of the VPs on HILIC across various serotypes showed VP3 variants, which elute before and after the main VP3 protein. These VP3 variants are likely either VP3 with oxidation or phosphorylation.[41] Although the oxidation and phosphorylation of VP3 have not been confirmed in this work, a prior study[41] confirmed that VP3 protein with oxidation and phosphorylation elutes after the main VP3 peak on the same HILIC column, following a similar method for several capsid serotypes. Cysteine residues are most susceptible to oxidation because of highly reactive sulfur groups.[46] The oxidation of SH to SOH, SO_2H, and SO_3H can lead to increased hydrophilicity of the viral protein, resulting in its later elution compared with the main VP3 capsid variant. Figure 5F shows that the more hydrophilic VP3 variant (VP 3.2) is more prominently seen in the full capsid fraction from AEX than in the empty capsid fractions. Figure 5G shows that this phenomenon is also seen for VP2, as the later eluting VP2 variant (VP2.1) is present in greater quantity among the full capsids and the E2 and E3 empty capsids fractions from AEX.
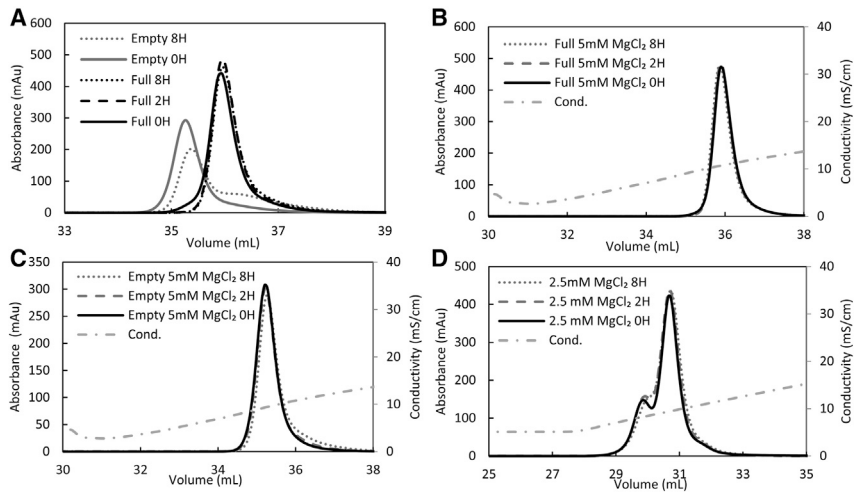
Figure 7. Changes in the chromatographic elution profiles (absorbance at 280 nm) seen after 0–8 h of extended binding in the presence of MgCl₂

UV absorbance at 280 nm is plotted on the left axis, and the conductivity trace (dash-dotted line) is plotted on the right axis. Purified empty and full capsids were bound separately onto the POROS XQ resin. (A and B) The elution chromatogram for empty and full capsids in the absence of MgCl₂ is shown in (A) and for full capsids in the presence of 5 mM MgCl₂ is shown in (B). The elution chromatogram of the empty capsid in the presence of 5 mM MgCl₂ is shown in (C). The elution chromatogram of a mixture of empty and full capsids in the presence of 2.5 mM MgCl₂ is shown in (D). The black solid, gray dashed, and gray dotted lines represent the chromatographic elution profiles after 0, 2, and 8 h of extended binding, respectively.

Furthermore, the VP1 variant (VP 1.1) that elutes earlier than the main VP1 protein, likely the N-terminal fragment,[41] is more prevalent in the empty capsids than the full capsids, as shown in Figure 5G. Last, the HILIC analysis presented across Figures 5E, 5F, and 5G shows that no significant differences are seen between capsids that were held on the column for 8 h vs. the control, revealing that for capsids with a given retention on AEX, no striking variation are seen across the VPs on HILIC. However, the capsids that retain differently on the AEX resin do show variation in the VP profiles, as shown in Figures 5H and 5I. Extended binding leads to an increasing percentage of the capsids retaining more strongly on the column. These strongly retaining capsids display a greater percentage of VP variants than capsids that bind weakly. For example, the strongly retaining capsid variants requiring more NaCl to elute constitute a greater percentage of VP 3.2 and V P3.3 proteins.

Apart from VP analysis on HILIC, the rAAVa capsids bound to the AEX resin for an extended period were also analyzed by size exclusion chromatography. Figure S4 shows that some aggregates (<0.5% by fluorescence detection) were seen in the full capsid fraction, and no aggregates were found in the empty capsid fractions. Extended binding of up to 8 h did not lead to an increase in the total percentage aggregate. However, for the post-full peak, extended binding led to a rise in the first high-molecular-weight (HMW) peak (2.1%–3.1%) and an accompanying drop (4.2%–2.7%) in the second HMW peak. Although no additional aggregates were generated for full rAAVa capsids, the existing aggregate formed a higher-order aggregate in the process of extended binding. Empty capsids of rAVVa did not form aggregates upon extended binding but are composed of capsid proteins with greater heterogeneity. We observe that extended binding of rAAVa onto the AEX column can increase the presence of VP variants (Figure 5) but not necessarily form aggregates detectable by SEC (Figure S4).

A shift in the empty capsid retention time and subsequent loss of resolution between the empty and full capsids is a major concern for AAV production. Compromised resolution between the empty and full capsids will result in lower-quality drug substances and greater product heterogeneity, which can raise product immunogenicity concerns. Therefore, a mitigation strategy to prevent such degradation was sought for rAAVa on POROS XQ resin. Glycerol did not significantly affect the on-column stability of the capsid. This finding is consistent with an earlier report of glycerol's inability to prevent aggregation upon dilution.[21] Upon careful inspection, a slightly broader right shoulder develops after an 8 h hold on the column in the presence of glycerol. An even broader shoulder is seen in the presence of 0.003% Kolliphor P188 after an 8 h hold, suggesting that Kolliphor P188 did not prevent the alteration of empty capsids in their adsorbed state, leading to a greater shift in their retention time. Although the adverse impact of Kolliphor P188 on empty capsids' on-column stability seen here has not been previously reported, Kolliphor P188 showed no effect on solution stability at low IS buffers.[29] On the other hand, a kosmotropic salt, $(NH_4)_2SO_4$, promotes the stability of adsorbed full capsids. Last, MgCl₂ was assessed, as it is widely used in AAV separation[21,25,29,47–49] to improve the resolution between the empty and full AAV capsids and promote capsid stability. The addition of 5 mM MgCl₂ effectively mitigated the on-column degradation of rAAVa capsids, as was similarly observed by Lavoie et al.,[37] but for up to 8 h in this study, potentially through stabilizing the hydrophobic interaction between the capsid proteins.

In a typical AAV purification process, a significant portion of capsids may remain bound to the AEX resin for a long time, mainly when the affinity eluate requires significant dilution, increasing the sample loading time onto the AEX column. The binding durations of 2–8 h explored in this work consist of time frames relevant to preparative AEX chromatography and extended conditions to fully assess the impact of on-column instability. Although the loading time for a monolith column could be shorter than 2 h, as it tolerates higher flow rates, a lengthy loading time may be unavoidable for the standard packed-bed columns, particularly in scenarios where loading volumes are large and delays time may be experienced because of unforeseeable process errors and deviations.

Our ability to purify empty and full capsids to greater than 90% purity allowed the separate assessment of their on-column stability. Adsorbed capsids, particularly empty ones, can be unstable across relevant pH, binding IS, and resin ligand density. Our findings show that capsids adsorbed to the AEX resin can change over time, resulting in shifts in retention time and a loss of resolution between empty and full capsids. Our data show that, in general, binding at lower IS is not favorable for capsid stability, regardless of whether the capsids are bound on a packed bed or monolith column. The adsorbed state instability of rAAVs is investigated and seen across various AEX media and ligand densities, demonstrating its prevalence. Going a step further, we revealed differences between empty and full capsid variants at the VP level. $MgCl_2$ is presented as an effective strategy to mitigate the impact of extended binding to ensure the maximum possible consistency in product quality is maintained throughout the polishing chromatography for empty and full capsids together and separately. Considering that AEX chromatography is the most scalable method for separating empty and full capsid, such a significant potential for a change in product quality must be considered, evaluated, and addressed during process development to help ensure product quality.

MATERIALS AND METHODS

rAAV capsids

Two (proprietary) recombinant AAV capsids of Spark Therapeutics were used in this work. The rAAV vectors were produced via the triple transfection method in HEK293 cells. The rAAVs were harvested 72 h post-transfection. The rAAVa and rAAVb capsids used for all experiments originated from one bioreactor each and were processed as a single stream through lysis, clarification, affinity capture, and AEX polishing. Mixtures of empty and full capsids are the affinity eluate process intermediate, in which the empty and full capsids were separated using our platform AEX method with >90% purity (not disclosed). The purity was confirmed using analytical AEX chromatography. Between 1×10^{12} and 1×10^{13} capsids were loaded onto the AEX chromatograph.

Preparative chromatography experiments

The preparative chromatography experiments were performed on an ÄKTA Avant 25 (Cytiva, Marlborough, MA) with UV and conductimetric detectors and a fraction collector. A fluorescence detector (RF-20A) from Shimadzu (Kyoto, Japan) was also paired with an ÄKTA Avant 25 workstation. The intrinsic fluorescence from rAAV capsids at excitation 280 nm and emission 350 nm was recorded along with the absorbance at 280 and 260 nm.

POROS resins of 50 μm particle size (POROS I, POROS XQ, and POROS HQ) were purchased from Thermo Fisher Scientific (Waltham, MA). Proprietary Q resins with varying ligand densities (low, medium, and high) were provided by Thermo Fisher Scientific. A monolith column of 1 mL volume (CIMmultus QA – 1.3 μm) was purchased from Sartorius BIA Separations (Göttingen, Germany). Omnifit glass columns (Omnifit, Diba Industries Inc.) of inside diameter (ID) 0.3 cm and length 10 cm (volume 0.7 mL) were slurry (50%) packed with various POROS resins. The physical properties of the

evaluated resins are provided in Table S1. All the chromatographic runs were carried out at a linear flow rate of 300 cm/h.

The columns were first equilibrated with buffer A (50 mM Tris [pH 7.5–9.0], 15–75 mM NaCl, at) on an ÄKTA Avant 25 chromatographic workstation. In addition, 0–5 mM $MgCl_2$, 5% glycerol, 0.003% Kolliphor P 188, or 15 mM $(NH_4)_2SO_4$ was added to the base buffer A in the respective experiments evaluating additives. Bind-and-elute measurements were performed by loading between 1×10^{12} and 1×10^{13} rAAV. The capsid stock solution of 150 mM IS was diluted on the chromatography workstation during sample application to match buffer A. The concentration range was chosen to keep the loading of rAAV capsid to approximately 10% of the total equilibrium binding capacity of the column. After loading, the columns were washed with buffer A, and the bound capsids were held for 0–8 h by pausing the pump flow to evaluate the impact of extended binding. Once the hold time was complete, the columns were washed with 50 mM Tris at pH 8.5 with 45 mM NaCl to ensure all elute pools were comparable, regardless of the variation in loading buffer A. The bound capsids were then eluted across a linear gradient of 0%–70% buffer B (50 mM Tris [pH 8.5], 300 mM NaCl) over 20 column volumes (CVs). Once the linear gradient was formed, 5 CVs of buffer B were passed through the column. Before reuse, the columns were stripped with 7 CVs of 100 mM acetate (pH 3.0) and 1 M NaCl and sanitized with 200 mM NaOH.

Analytical chromatography

CIMac AAV full/empty 0.1 mL analytical column (1.3 μm) was purchased from Sartorius BIA Separations. XBridge Protein BEH SEC Column, 450 Å, 2.5 μm, 4.6 × 150 mm, was purchased from Waters (Milford, MA).

Empty and full rAAV capsids were quantified using CIMac AAV full/empty 0.1 mL analytical column (1.3 μm) (BIA Separations) connected to an ACQUITY UPLC H-Class BIO system from Waters. The UPLC is equipped with a photodiode array and fluorescence detectors. Empty and full capsid peaks were identified using the 260/280 nm absorbance ratio, while their relative concentrations were determined using the fluorescence signal at excitation and emission of 280 and 350 nm, respectively. The solutions used in the analytical AEX method were as follows: A: 20 mM Tris (pH 9) + 5 mM $MgCl_2$; B: 20 mM Tris (pH 9) + 300 mM NaCl + 5 mM $MgCl_2$; C: 20 mM acetic acid + 1 M NaCl; D: water.

Aggregate quantification was achieved using XBridge Protein BEH SEC Column, 450 Å, 2.5 μm, 4.6 × 150 mm column (Waters) connected to the UPLC. The mobile phase was 15 mM phosphate (pH 7.0) + 500 mM NaCl.

Capsid viral proteins were also analyzed on the UPLC equipped with a fluorescence detector using Waters ACQUITY UPLC Glycoprotein Amide column (300 Å, 1.7 μm, 2.1 × 150 mm) following the HILIC method outlined by Liu et al.[41] The mobile phases used were as follows: A: 0.1% (v/v) trifluoroacetic acid in water; and B: 0.1% (v/v)

trifluoroacetic acid in acetonitrile at a column temperature of 60°C. AAV samples of 1 μL each were injected into the column without sample preparation or dilution. The column was equilibrated and washed at 85% B for 0.5 min, followed by a second wash at 70% B for another 0.5 min. The sample was then eluted over a gradient of 70%–64% B over 16 min. The VP1, VP2, and VP3 capsid proteins and their variants were identified on the fluorescence chromatogram following the order outlined in Liu et al. Once the VP proteins were identified, the method was further optimized for better separation, as outlined in the supplemental information.

DATA AND CODE AVAILABILITY

The authors confirm that the data supporting the findings of this study are available within the article and/or its supplemental information.

SUPPLEMENTAL INFORMATION

Supplemental information can be found online at https://doi.org/10.1016/j.omtm.2023.101112.

AUTHOR CONTRIBUTIONS

Conceptualization, O.K. and V.K.; methodology, O.K. and V.K.; investigation, O.K. and V.K.; writing – original draft, O.K. and V.K.; writing – review & editing, O.K., V.K., and M.J.; resources, O.K. and M.J.

DECLARATION OF INTERESTS

The authors declare no competing interests.

REFERENCES

1. Dunbar, C.E., High, K.A., Joung, J.K., Kohn, D.B., Ozawa, K., and Sadelain, M. (2018). Gene therapy comes of age. Science, 359. https://doi.org/10.1126/SCIENCE.AAN4672/ASSET/4136786F-5233-4623-8B57-522F753667A6/ASSETS/GRAPHIC/359_AAN4672_F3.JPEG.

2. Bennett, J., Ashtari, M., Wellman, J., Marshall, K.A., Cyckowski, L.L., Chung, D.C., McCague, S., Pierce, E.A., Chen, Y., Bennicelli, J.L., et al. (2012). Gene therapy: AAV2 gene therapy readministration in three adults with congenital blindness. Sci. Transl. Med. 4, 120ra15. https://doi.org/10.1126/SCITRANSLMED.3002865/SUPPL_FILE/4-120RA15_SM.PDF.

3. Chowdary, P., Shapiro, S., Makris, M., Evans, G., Boyce, S., Talks, K., Dolan, G., Reiss, U., Phillips, M., Riddell, A., et al. (2022). Phase 1–2 Trial of AAVS3 Gene Therapy in Patients with Hemophilia B. N. Engl. J. Med. 387, 237–247. https://doi.org/10.1056/NEJMOA2119913/SUPPL_FILE/NEJMOA2119913_DATA-SHARING.PDF.

4. Lykken, E.A., Shyng, C., Edwards, R.J., Rozenberg, A., and Gray, S.J. (2018). Recent progress and considerations for AAV gene therapies targeting the central nervous system. J. Neurodev. Disord. 10, 16. https://doi.org/10.1186/S11689-018-9234-0.

5. Qu, Y., Liu, Y., Noor, A.F., Tran, J., and Li, R. (2019). Characteristics and advantages of adeno-associated virus vector-mediated gene therapy for neurodegenerative diseases. Neural Regen. Res. 14, 931–938. https://doi.org/10.4103/1673-5374.250570.

6. ASGCT/Pharma Intelligence Quarterly Report: Q1 2022 L Pharma Intelligence https://pharmaintelligence.informa.com/asgct-report?gclid=Cj0KCQjw08aYBhDlARIsAA_gb0cFOlHsHs_iLGQpxZoU9bDEyRaUfYdP0iwfQXhcFAX7T80VkFvuw-YaAk7NEALw_wcB.

7. Wang, D., Tai, P.W.L., and Gao, G. (2019). Adeno-associated virus vector as a platform for gene therapy delivery. Nat. Rev. Drug Discov. 18, 358–378. https://doi.org/10.1038/S41573-019-0012-9.

8. George, L.A., Monahan, P.E., Eyster, M.E., Sullivan, S.K., Ragni, M.V., Croteau, S.E., Rasko, J.E.J., Recht, M., Samelson-Jones, B.J., MacDougall, A., et al. (2021). Multiyear Factor VIII Expression after AAV Gene Transfer for Hemophilia A. N. Engl. J. Med. 385, 1961–1973. https://doi.org/10.1056/NEJMOA2104205/SUPPL_FILE/NEJMOA2104205_DATA-SHARING.PDF.

9. Nathwani, A.C., Tuddenham, E.G.D., Rangarajan, S., Rosales, C., McIntosh, J., Linch, D.C., Chowdary, P., Riddell, A., Pie, A.J., Harrington, C., et al. (2011). Adenovirus-Associated Virus Vector–Mediated Gene Transfer in Hemophilia B. N. Engl. J. Med. 365, 2357–2365. https://doi.org/10.1056/NEJMOA1108046.

10. Mingozzi, F., Anguela, X.M., Pavani, G., Chen, Y., Davidson, R.J., Hui, D.J., Yazicioglu, M., Elkouby, L., Hinderer, C.J., Faella, A., et al. (2013). Overcoming Preexisting Humoral Immunity to AAV Using Capsid Decoys. Sci. Transl. Med. 5, 194ra92. https://doi.org/10.1126/SCITRANSLMED.3005795.

11. Wright, J.F. (2014). AAV Empty Capsids: For Better or for Worse? Mol. Ther. 22, 1–2. https://doi.org/10.1038/MT.2013.268.

12. Leborgne, C., Barbon, E., Alexander, J.M., Hanby, H., Delignat, S., Cohen, D.M., Collaud, F., Muraleetharan, S., Lupo, D., Silverberg, J., et al. (2020). IgG-cleaving endopeptidase enables in vivo gene therapy in the presence of anti-AAV neutralizing antibodies. Nat. Med. 26, 1096–1101. https://doi.org/10.1038/s41591-020-0911-7.

13. Calcedo, R., and Wilson, J.M. (2013). Humoral Immune Response to AAV. Front. Immunol. 4, 341. https://doi.org/10.3389/FIMMU.2013.00341.

14. Mingozzi, F., Maus, M.V., Hui, D.J., Sabatino, D.E., Murphy, S.L., Rasko, J.E.J., Ragni, M.V., Manno, C.S., Sommer, J., Jiang, H., et al. (2007). CD8+ T-cell responses to adeno-associated virus capsid in humans. Nat. Med. 13, 419–422. https://doi.org/10.1038/nm1549.

15. Gao, K., Li, M., Zhong, L., Su, Q., Li, J., Li, S., He, R., Zhang, Y., Hendricks, G., Wang, J., and Gao, G. (2014). Empty Virions In AAV8 Vector Preparations Reduce Transduction Efficiency And May Cause Total Viral Particle Dose-Limiting Side-Effects. Mol. Ther. Methods Clin. Dev. 1, 20139. https://doi.org/10.1038/MTM.2013.9.

16. Urabe, M., Xin, K.Q., Obara, Y., Nakakura, T., Mizukami, H., Kume, A., Okuda, K., and Ozawa, K. (2006). Removal of empty capsids from type 1 adeno-associated virus vector stocks by anion-exchange chromatography potentiates transgene expression. Mol. Ther. 13, 823–828. https://doi.org/10.1016/J.YMTHE.2005.11.024.

17. Qu, G., Bahr-Davidson, J., Prado, J., Tai, A., Cataniag, F., McDonnell, J., Zhou, J., Hauck, B., Luna, J., Sommer, J.M., et al. (2007). Separation of adeno-associated virus type 2 empty particles from genome containing vectors by anion-exchange column chromatography. J. Virol. Methods 140, 183–192. https://doi.org/10.1016/J.JVIROMET.2006.11.019.

18. Nass, S.A., Mattingly, M.A., Woodcock, D.A., Burnham, B.L., Ardinger, J.A., Osmond, S.E., Frederick, A.M., Scaria, A., Cheng, S.H., and O'riordan, C.R. (2018). Universal Method for the Purification of Recombinant AAV Vectors of Differing Serotypes. https://doi.org/10.1016/j.omtm.2017.12.004.

19. Brument, N., Morenweiser, R., Blouin, V., Toublanc, E., Raimbaud, I., Chérel, Y., Folliot, S., Gaden, F., Boulanger, P., Kroner-Lux, G., et al. (2002). A Versatile and Scalable Two-Step Ion-Exchange Chromatography Process for the Purification of Recombinant Adeno-associated Virus Serotypes-2 and -5. Mol. Ther. 6, 678–686. https://doi.org/10.1006/MTHE.2002.0719.

20. Burova, E., and Ioffe, E. (2005). Chromatographic purification of recombinant adeno-viral and adeno-associated viral vectors: methods and implications. Gene Ther. 12, S5–S17. https://doi.org/10.1038/sj.gt.3302611.

21. Wang, C., Mulagapati, S.H.R., Chen, Z., Du, J., Zhao, X., Xi, G., Chen, L., Linke, T., Gao, C., Schmelzer, A.E., and Liu, D. (2019). Developing an Anion Exchange Chromatography Assay for Determining Empty and Full Capsid Contents in AAV6.2. Mol. Ther. Methods Clin. Dev. 15, 257–263. https://doi.org/10.1016/J.OMTM.2019.09.006.

22. Kaludov, N., Handelman, B., and Chiorini, J.A. (2002). Scalable purification of adeno-associated virus type 2, 4, or 5 using ion-exchange chromatography. Hum. Gene Ther. 13, 1235–1243. https://doi.org/10.1089/104303402320139014.

23. Zolotukhin, S., Byrne, B.J., Mason, E., Zolotukhin, I., Potter, M., Chesnut, K., Summerford, C., Samulski, R.J., and Muzyczka, N. (1999). Recombinant adeno-associated virus purification using novel methods improves infectious titer and yield. Gene Ther. 6, 973–985. https://doi.org/10.1038/sj.gt.3300938.

24. Davidoff, A.M., Ng, C.Y.C., Sleep, S., Gray, J., Azam, S., Zhao, Y., McIntosh, J.H., Karimipoor, M., and Nathwani, A.C. (2004). Purification of recombinant adeno-associated virus type 8 vectors by ion exchange chromatography generates clinical grade vector stock. J. Virol. Methods 121, 209–215. https://doi.org/10.1016/J.JVIROMET.2004.07.001.

25. Dickerson, R., Argento, C., Pieracci, J., and Bakhshayeshi, M. (2021). Separating Empty and Full Recombinant Adeno-Associated Virus Particles Using Isocratic Anion Exchange Chromatography. Biotechnol. J. 16, 2000015. https://doi.org/10.1002/BIOT.202000015.

26. Lock, M., Alvira, M.R., and Wilson, J.M. (2012). Analysis of particle content of recombinant adeno-associated virus serotype 8 vectors by ion-exchange chromatography. Hum. Gene Ther. Methods 23, 56–64. https://doi.org/10.1089/HGTB.2011.217.

27. Yang, Y., Su, Z., Ma, G., and Zhang, S. (2020). Characterization and stabilization in process development and product formulation for super large proteinaceous particles. Eng. Life Sci. 20, 451–465. https://doi.org/10.1002/ELSC.202000033.

28. Yang, Y., Song, Y., Lin, X., Li, S., Li, Z., Zhao, Q., Ma, G., Zhang, S., and Su, Z. (2020). Mechanism of bio-macromolecule denaturation on solid-liquid surface of ion-exchange chromatographic media – A case study for inactivated foot-and-mouth disease virus. J. Chromatogr. B 1142, 122051. https://doi.org/10.1016/J.JCHROMB.2020.122051.

29. Wright, J.F., Le, T., Prado, J., Bahr-Davidson, J., Smith, P.H., Zhen, Z., Sommer, J.M., Pierce, G.F., and Qu, G. (2005). Identification of factors that contribute to recombinant AAV2 particle aggregation and methods to prevent its occurrence during vector purification and formulation. Mol. Ther. 12, 171–178. https://doi.org/10.1016/J.YMTHE.2005.02.021.

30. Wang, W., and Roberts, C.J. (2013). Non-Arrhenius Protein Aggregation. AAPS J. 15, 840–851. https://doi.org/10.1208/S12248-013-9485-3.

31. Drenski, M., Brader, M., Alston, R., and biochemistry, W.R.-A. (2013). Undefined Monitoring Protein Aggregation Kinetics with Simultaneous Multiple Sample Light Scattering (Elsevier).

32. Kayser, V., Chennamsetty, N., Voynov, V., et al. (2011). Undefined Evaluation of a Non-arrhenius Model for Therapeutic Monoclonal Antibody Aggregation (Elsevier).

33. Brummitt, R., Nesta, D., sciences, C.R.-J. Of Pharmaceutical, and 2011, Undefined Predicting Accelerated Aggregation Rates for Monoclonal Antibody Formulations, and Challenges for Low-Temperature Predictions. Elsevier.

34. Rodrigues, G.A., Shalaev, E., Karami, T.K., Cunningham, J., Slater, N.K.H., and Rivers, H.M. Pharmaceutical Development of AAV-Based Gene Therapy Products for the Eye. https://doi.org/10.1007/s11095-018-2554-7.

35. Wu, J., and Heger, C. (2022). Establishment of a platform imaged capillary isoelectric focusing (icIEF) characterization method for adeno-associated virus (AAV) capsid proteins. Green Analytical Chemistry 3, 100027. https://doi.org/10.1016/J.GREEAC.2022.100027.

36. Giles, A., Sims, J., Turner, K., and Therapy, L.G.-M. (2018). Undefined Deamidation of Amino Acids on the Surface of Adeno-Associated Virus Capsids Leads to Charge Heterogeneity and Altered Vector Function (Elsevier).

37. Lavoie, R.A., Zugates, J.T., Cheeseman, A.T., Teten, M.A., Ramesh, S., Freeman, J.M., Swango, S., Fitzpatrick, J., Joshi, A., Hollers, B., et al. (2023). Enrichment of adeno-associated virus serotype 5 full capsids by anion exchange chromatography with dual salt elution gradients. Biotechnol. Bioeng. 120, 2953–2968. https://doi.org/10.1002/BIT.28453.

38. Sommer, J.M., Smith, P.H., Parthasarathy, S., Isaacs, J., Vijay, S., Kieran, J., Powell, S.K., McClelland, A., and Wright, J.F. (2003). Quantification of adeno-associated virus particles and empty capsids by optical density measurement. Mol. Ther. 7, 122–128. https://doi.org/10.1016/S1525-0016(02)00019-9.

39. McIntosh, N.L., Berguig, G.Y., Karim, O.A., Cortesio, C.L., De Angelis, R., Khan, A.A., Gold, D., Maga, J.A., and Bhat, V.S. (2021). Comprehensive characterization and quantification of adeno associated vectors by size exclusion chromatography and multi angle light scattering. Sci. Rep. 11, 3012. https://doi.org/10.1038/s41598-021-82599-1.

40. Werle, A.K., Powers, T.W., Zobel, J.F., Wappelhorst, C.N., Jarrold, M.F., Lyktey, N.A., Sloan, C.D.K., Wolf, A.J., Adams-Hall, S., Baldus, P., and Runnels, H.A. (2021). Comparison of analytical techniques to quantitate the capsid content of adeno-associated viral vectors. Mol. Ther. Methods Clin. Dev. 23, 254–262. https://doi.org/10.1016/J.OMTM.2021.08.009.

41. Liu, A.P., Patel, S.K., Xing, T., Yan, Y., Wang, S., and Li, N. (2020). Characterization of Adeno-Associated Virus Capsid Proteins Using Hydrophilic Interaction Chromatography Coupled with Mass Spectrometry. J. Pharm. Biomed. Anal. 189, 113481. https://doi.org/10.1016/J.JPBA.2020.113481.

42. Du, Y., Walsh, A., Ehrick, R., Xu, W., May, K., and Liu, H. (2012). Chromatographic analysis of the acidic and basic species of recombinant monoclonal antibodies. mAbs 4, 578–585. https://doi.org/10.4161/MABS.21328.

43. Teshima, G., Li, M.X., Danishmand, R., Obi, C., To, R., Huang, C., Kung, J., Lahidji, V., Freeberg, J., Thorner, L., and Tomic, M. (2011). Separation of oxidized variants of a monoclonal antibody by anion-exchange. J. Chromatogr. A 1218, 2091–2097. https://doi.org/10.1016/J.CHROMA.2010.10.107.

44. He, X.Z., Powers, T.W., Huang, S., Liu, Z., Shi, H., Orlet, J.D., Mo, J.J., Srinivasan, S., Jacobs, S., Zhang, K., et al. (2023). Development of an icIEF Assay for Monitoring AAV Capsid Proteins and Application to Gene Therapy Products. https://doi.org/10.1016/j.omtm.2023.03.002.

45. Wörner, T.P., Bennett, A., Habka, S., Snijder, J., Friese, O., Powers, T., Agbandje-McKenna, M., and Heck, A.J.R. (2021). Adeno-associated virus capsid assembly is divergent and stochastic. Nat. Commun. 12, 1–9. https://doi.org/10.1038/s41467-021-21935-5.

46. Davies, M.J. (2016). Protein oxidation and peroxidation. Biochem. J. 473, 805–825. https://doi.org/10.1042/BJ20151227.

47. Gagnon, P., Goričar, B., Prebil, S.D., Jug, H., Leskovec, M., and Štrancar, A. Separation of Empty and Full Adeno-Associated Virus Capsids from a Weak Anion Exchanger by Elution with an Ascending pH Gradient at Low Ionic Strength.

48. Gagnon, P., Goricar, B., Mencin, N., Zvanut, T., Peljhan, S., Leskovec, M., and Strancar, A. (2021). Multiple-Monitor HPLC Assays for Rapid Process Development, In-Process Monitoring, and Validation of AAV Production and Purification. Pharmaceutics 13, 113–114. https://doi.org/10.3390/PHARMACEUTICS13010113.

49. Gagnon, P., Leskovec, M., Prebil, S.D., Žigon, R., Štokelj, M., Raspor, A., Peljhan, S., and Štrancar, A. (2021). Removal of empty capsids from adeno-associated virus preparations by multimodal metal affinity chromatography. J. Chromatogr. A 1649, 462210. https://doi.org/10.1016/J.CHROMA.2021.462210.